POLITECNICO DI TORINO
Repository ISTITUZIONALE

Use of gelatin/nanocellulose compacted polyelectrolyte complexes to upcycle collagen-rich fibers into lightweight, strong, insulating and fire-safe fiber networks

Original
Use of gelatin/nanocellulose compacted polyelectrolyte complexes to upcycle collagen-rich fibers into lightweight, strong, insulating and fire-safe fiber networks / Abba, L., Mascolo, R., Florio, C., Fina, A., Carosio, F.. - In: POLYMER DEGRADATION AND STABILITY. - ISSN 0141-3910. - 252:(2026), pp. 1-10. [10.1016/j.polymdegradstab.2026.112300]

Availability:
This version is available at: 11583/3017227 since: 2026-10-30T09:25:27Z

Publisher:
Elsevier

Published
DOI:10.1016/j.polymdegradstab.2026.112300

Terms of use:

This article is made available under terms and conditions as specified in the corresponding bibliographic description in the repository

Publisher copyright

(Article begins on next page)

07 November 2026

Polymer Degradation and Stability 252 (2026) 112300

Contents lists available at ScienceDirect

Polymer Degradation and Stability

journal homepage: www.journals.elsevier.com/polymer-degradation-and-stability

Use of gelatin/nanocellulose compacted polyelectrolyte complexes to upcycle collagen-rich fibers into lightweight, strong, insulating and fire-safe fiber networks

Lorenza Abbà [a], Rosario Mascolo [b], Claudia Florio [b], Alberto Fina [a], Federico Carosio [a,*]

[a] Dipartimento di Scienza Applicata e Tecnologia, Politecnico di Torino-Alessandria Campus, Viale Teresa Michel 5, 15121, Alessandria, Italy
[b] Stazione Sperimentale per l'Industria delle Pelli e delle materie concianti-SSIP (Italian Leather Research Institute), Comprensorio Olivetti, Via Campi Flegrei, 34, 80078 Pozzuoli, NA, Italy

ARTICLE INFO

Keywords:
Polyelectrolyte complexes
Collagen-rich fibers
Upcycling
Lightweight materials
Flame retardancy

ABSTRACT

The upcycling of collagen-rich waste fibers into lightweight materials represents a potential opportunity to fulfill current societal demands for a circular bioeconomy. With this objective, this paper reports a novel strategy that relies on the use of polyelectrolyte complexes beyond their conventional application fields. To this aim, compacted polyelectrolyte complexes (CoPECs) encompassing gelatin and nanocellulose are here used, for the first time, as a structural matrix to upcycle collagen-rich fibers into mechanically robust, insulating and fire safe fiber networks. The effects of pH complexing conditions on the strength of the dry CoPECs were investigated highlighting optimal mechanical properties at pH 6. This enabled the use of CoPECs for the preparation of fiber networks characterized by a wide range of compositions (fiber content up to 75%) and densities (50 and 90 kg/m^3). The CoPECs matrix stabilizes and improves the formation of strong fiber-fiber joints conferring structural integrity to the networks with compressive strengths at 10% deformation up to 0.102 MPa. The thermal conductivity can be as low as 0.043 W/(m·K). The intrinsic flame retardant characteristics of collagen-rich fibers allow to easily stop flame propagation during flammability tests. When exposed to the heat flux of a developing fire (50 kW/m^2) these materials can achieve low heat and smoke release if compared with high performing state-of-the-art solutions. This paper discloses a novel use of CoPECs for the production of advanced materials capable of balancing sustainability and functional properties while also providing a greener and safer alternative to conventional foams for transportation or building applications.

1. Introduction

The increasing global concern about the depletion of fossil resources and the production of high amount of plastic wastes has fostered the development of functional green materials with reduced environmental impact [1]. Composite materials encompassing bio-sourced fillers can represent a possible solution toward a more sustainable economy [2]. Indeed, in the last decades, natural fibers from both plant and animal sources, have gained a lot of attention in the material science field thanks to their low cost, large availability and biodegradability [3,4]. Among them leather shavings, a waste from tannery processes, might represent a good candidate for the development of bio-sourced composite materials. Indeed, while leather production is estimated to be about 23 billion square feet annually [5], the sector is currently facing increasing challenges linked to the production of substantial amounts of wastewater, sludge, and solid waste [6–8]. These latter are therefore the object of current technological efforts aimed at either their limitation or valorization [9–12]. Being generated after the tanning process, leather shavings represent a major area of concern since they are tailored to withstand biological degradation. Therefore, traditional disposing methods such as landfilling and incineration typically result in a waste of resources while potentially raising environmental issues. As addressing these latter might significantly impact production costs, the leather industry is now seeking for green and easily applicable technologies that enable the recycling or upcycling of wastes into functional materials. In order to be impactful, such innovations should not only mitigate environmental issues but also produce novel circular materials therefore enabling a more sustainable and valuable manufacturing [13,

* Corresponding author.
E-mail address: federico.carosio@polito.it (F. Carosio).

https://doi.org/10.1016/j.polymdegradstab.2026.112300
Received 9 May 2026; Received in revised form 17 June 2026; Accepted 22 June 2026
Available online 22 June 2026
0141-3910/© 2026 The Authors. Published by Elsevier Ltd. This is an open access article under the CC BY license (http://creativecommons.org/licenses/by/4.0/).

14]. Within this context, the upcycling of leather shavings to produce functional materials represent a relevant challenge toward the reduction of the environmental impact.

Leather shavings are rich in proteins, especially collagen. Collagen possess a unique hierarchical structure organized into a multistage architecture comprising fibrils, fibers and fiber bundles until the final structure of a fiber is reached [15,16]. Several studies proposed different strategies for the valorization of the solid tannery wastes. Protein-rich waste could be hydrolyzed to obtain collagen or gelatin for cosmetic or biomedical applications [17,18]. By chemical treatment chromium could be recovered and recycled for the preparation of pigments or reintroduced into the leather making process [19,20]. In addition, leather shavings, thanks to the high number of polar groups, have been applied for the removal of organic compound and metal ions [21,22]. Beside processes aimed at extracting chemical, solid wastes could be directly used to make composite materials. Dos Santos et al. used leather wastes as a filler into expanded styrene-butadiene rubber to make thermal and acoustic insulator material as an alternative to synthetic rubbers [23]. Collagen fibers have also been used as flame retardant filler for natural rubber modification [24]. Li et al. proposed to use leather wastes, poly(vinyl alcohol) and polyaniline to make aerogel with enhanced mechanical, flame retardancy and electromagnetic interference shielding performances [25]. In particular, the field of lightweight materials represent a great opportunity for the up-cycling of fiber wastes. Foamed materials are widely used for different applications, from the packaging to the construction sector [26,27]. Within this context, it is well known that traditional petroleum-derived foams (like polyurethane or polystyrene foams) present sustainability and fire-safety problems [28]. As environmental consciousness rises, the use of animal fibers to make functional materials can represent a valuable solution. However, the production of stable, low density 3-dimensional structures based on natural fibers is still challenging. The use of bio-sourced polyelectrolyte complexes (PECs) in combination with freeze-drying could offer a possible solution. The electrostatic complexation of bio-based components is often considered as an environmentally friendly approach for the development of novel materials. Indeed, the process is typically performed in aqueous media without the use of harsh chemicals or conditions and is straightforward to scale up [29]. Stable PECs can be produced by mixing water-based solutions/suspensions of oppositely charged polycations and polyanions in controlled conditions [30]. The primary interaction is the electrostatic attraction occurring between oppositely charged poly-ions; however, additional interactions such as hydrogen bonding, ionic dipole forces and hydrophobic interactions may also contribute to PECs formation [31]. At a macroscopic level, the process results into a phase separation into a dilute supernatant phase and a dense polymer-rich phase. Depending on the interactions between the polyelectrolyte chains, the dense phase could be a liquid-like coacervate or a solid-like precipitate. The nature and the properties of the PECs could be influenced and controlled by different parameters like charge density, pH, ionic strength or temperature [32–34]. Since the dense polymer-rich phase contains a significant amount of water, it can be further densified by ultracentrifugation [35], extrusion [36], hot-pressing [37] or sedimentation [38]. The obtained dense solid are called compacted PECs (CoPECs) [39]. Thanks to the strong interactions occurring at molecular level, PECs often can display a unique set of properties (e.g., high mechanical strength, flame retardancy and thermal stability) [40]. Recent studies on PECs formation and processing conditions have therefore opened up to many applications in different fields [29]. Indeed, PECs have been used as biosorbents [41], self-healing hydrogels [42], carrier for drugs [43] or thin films/membranes [44,45]. In addition, the formation of stable PECs or CoPECs often enables easy and straightforward processing options for their exploit as coatings or self-standing membranes. For example, the gel produced by combining branched polyethylenimine and cellulose nanocrystals allowed the deposition of the PECs as FR coating on cotton by a simple doctor blading approach [46]. Beside the use as coatings, PECs or CoPECs incorporating functional particles have attracted great interest as potential route for the preparation of composite materials. For example, Schlenoff et al. developed a nanocomposite based on poly(styrenesulfonate) and poly(diallyldimethylammonium) PECs embedding iron oxide nanoparticles with superparamagnetic properties [47]. Similarly, PECs hybrid composite membranes filled with silica and carbon nanotubes were synthesized for pervaporation applications [48]. Despite recent publications on PECs-based composites, to the best of our knowledge, there are no reports regarding the use of PECs as a matrix for the production of lightweight porous materials.

To this aim, the main purpose of this work is to propose an easy and straightforward approach capable of combining bio-sourced PECs and the up-cycling of tannery fibrous waste into functional, lightweight and flame retardant fiber networks suitable for thermal insulation applications. Gelatin (GEL) and carboxymethylated cellulose nanofibers (CNF) were employed as PECs components. Collagen-rich leather shavings were used as functional fibers to be included into the PECs matrix. Fig. 1 reports the schematization of the procedure employed for the production of the lightweight porous fiber network structure developed in this paper.

In the material design, the PECs act like a matrix and a binder between the fibers ensuring the mechanical integrity of the sample while the fibers primarily contribute to the flame retardancy properties of the network. The optimal complexing conditions capable of yielding stable and mechanically strong CoPECs upon freeze-drying were thoroughly investigated by infrared spectroscopy, scanning electron microscopy (SEM) and compression tests. Lightweight and functional fiber networks were then prepared by incorporating the collagen-rich fibers in the CoPECs targeting different compositions (50/50 and 25/75 CoPECs/fibers) and densities (50 and 90 kg/m^3). The morphology was evaluated by scanning electron microscopy (SEM). The mechanical and insulating properties were measured through compression and thermal conductivity tests, respectively. The fire safety of the prepared fiber networks was assessed by flammability (in horizontal and vertical configurations) and forced combustion tests (cone calorimetry test at 50 kW/m^2). The fire performances were benchmarked against those of high performing materials from the literature background.

2. Materials and method

2.1. Materials

Vegetable tanned bovine shavings were reduced into fibers by means of a Pulverisette 19 grinder (Fritsch, Germany) fitted with a 1.5 mm sieve [49]. Gelatin from cold water fish skin (GEL) and acetic acid were purchased from Sigma Aldrich (Milano, IT). Carboxymethylated cellulose nanofibers (CNF) were purchased from RISE (Sweden) as approx. 2 wt% gel. Gelatin was dissolved at 1 wt% in deionized water for 1 h while CNF suspension was prepared by diluting the gel up to 0.25 wt% concentration and kept under magnetic stirring overnight. The so-prepared CNF suspension was then homogenized for 10 min at speed 9500 rpm using Ultra-Turrax high-speed homogenizer based on the rotor-stator principle (Ultra-Turrax T25 basic, IKA-WERKE, Staufen, Germany). The pH of gelatin was adjusted to 4, 5 and 6 using pure acetic acid or 1 M NaOH solution whereas the pH of CNF was kept unmodified at 7. All the solutions were prepared with 18.2 MΩ deionized water supplied by a Q20 Millipore system (Milano, Italy).

2.2. Polyelectrolyte complexes and fiber network preparation

The GEL solution (at different pH) and the CNF suspension were mixed in equal volume and kept under magnetic stirring for 20 min. Gelatin pH was modified with acetic acid or sodium hydroxide solutions (1 M) in order to obtain the desired pH. The prepared suspensions were then centrifuged (Eppendorf, Centrifuge 5702) for 10 min at 4400 rpm

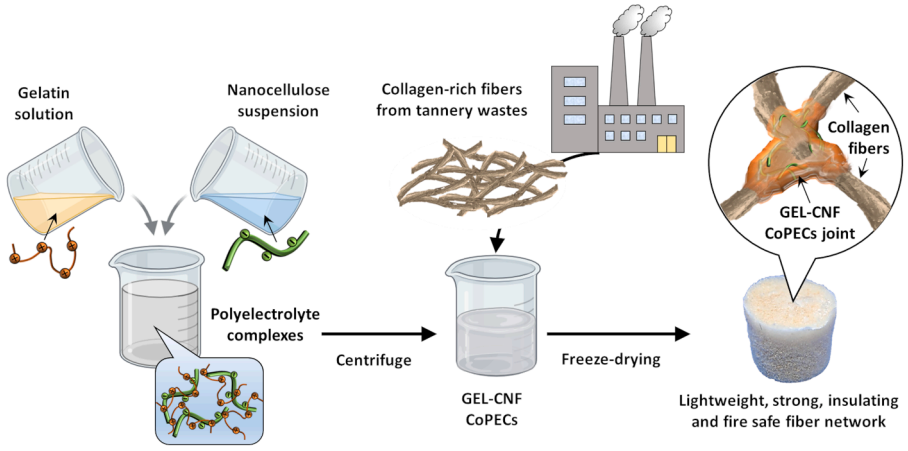


Fig. 1. Schematic representation of the approach developed in this paper. First gelatin solution and CNF suspension were mixed together and, after complexation, the suspension was centrifuged in order to obtain the polymer-rich concentrated phase (CoPECs). The GEL-CNF gel was mixed with collagen fibers and then freeze-dried to obtain the porous lightweight fiber networks.

(Fig. S1). The precipitate (in the form of a gel, CoPECs) was collected and the supernatant was subsequently removed. The so obtained GEL/CNF CoPECs gel had a dry content of 4 wt% (evaluated by drying the PECs in a ventilated oven at 80 °C). CoPECs prepared at pH 4, 5 and 6 were frozen at a temperature of −40 °C for 12 h and then freeze-dried for 48 h using a vacuum freeze-dryer (Toption TOPT-10A, vacuum freeze-dryer) to produce cylindrical samples in order to evaluate the dry-CoPECs mechanical properties.

Before preparing the fiber networks, the collagen-rich fibers were dried in the oven at 60 °C for at least 3 h in order to remove the moisture. After that the CoPECs gel and the dried fibers were mixed in order to obtain a weight ratio of 50:50 and 25:75 between the fibers and the complex (based on the dry content of the gel). Deionized water was added in different amount in order to achieve a final density of 50 or 90 kg/m^3. The name of the samples and the calculated densities are collected in Table S1. Finally, the mixture was mechanically stirred for 5 min at low speed to produce a stable suspension. The resulting suspension was subsequently cast into silicone molds (size related to the characterization techniques as described in chapter 2.3), froze at a temperature of −40 °C for 12 h and then freeze-dried for 48 h using a vacuum freeze-dryer (Toption TOPT-10A, vacuum freeze-dryer) to produce the fiber networks. In the following, the samples are coded reporting the composition (CoPECs/fibers) and density (d): for example, a sample coded 25/75 d50 refers to a fiber network encompassing 25 wt % CoPECs and 75 wt% fibers with a density of 50 kg/m^3.

2.3. Characterization techniques

Attenuated total reflection (ATR) Fourier Transform infrared (FTIR) spectroscopy spectra of fibers, dried complexes and fiber networks were collected at room temperature, in the range of 4000 - 400 cm^{-1} (16 scans, 4 cm^{-1} resolution) with an ATR- FTIR spectrometer (Frontier, Perkin Elmer, Italy) equipped with a diamond crystal.

Surface morphology of the samples was investigated, after gold sputtering, using Scanning Electron Microscopy (SEM) on a Zeiss EVO 15 model.

The sample density was calculated as the ratio between the weight and the volume of cylindrical specimens. The specimens were weighted using an analytical balance (RADWAG, Poland) and the dimensions were measured using a high-resolution caliper. Samples were dried overnight in an oven at 60 °C before weight measurement. The calculated density was the average of five samples.

Mechanical properties were evaluated by compressing cylindrical samples of approx. 20 mm diameter and 20 mm height using a dynamometer (Instron 5966, 2 kN cell, Canton, MA). The samples were compressed between two horizontal plates at a constant rate of 10 mm/min. Before the test the samples were stored into a climatic chamber at 23.0 ± 0.1 °C and 50.0 ± 0.1%RH for 48 h.

Thermal conductivity was evaluated by a transient plane heat source method (ISO 22007-2) using TPS 2500S instrument by Hot Disk AB (Göteborg, Sweden) equipped with a Kapton sensor (radius 9.868 mm). The measuring setup was placed in a container and immersed in a silicone oil bath (Haake A40, Thermo Scientific Inc., Waltham, MA, USA) equipped with a temperature controller (Haake AC200, Thermo Scientific Inc., Waltham, MA, USA) to maintain the temperature at 23.00 ± 0.01 °C. Square samples of 50 mm x 50 mm x 15 mm thickness were tested. Before the test, specimens were stored in a climatic chamber at 23.0 ± 0.1 °C and 50.0 ± 0.1%RH for 24 h.

The flammability of samples was performed both in horizontal and vertical configurations. The sample (50 mm x 20 mm x 10 mm) was ignited by a 20 mm blue methane flame (flame application: 2 × 6 s). The test was repeated at least three times for each formulation and during the test the ability to stop flame spread and final residue (%) were evaluated. Prior the test, samples were conditioned in a climatic chamber (23.0 ± 0.1 °C, 50.0 ± 0.1%RH) for at least 48 h.

The combustion behavior of the samples was investigated by cone calorimetry (GA01, ISO 5660, Noselab Ats, Italy). Square sample (50 mm x 50 mm x 15 mm) were placed under 50 kW/m^2 heat flux and the following parameters were registered: Time to Ignition (TTI, (s)), peak of Heat Release Rate (pkHRR, (kW/m^2)), Total Heat Release (THR, (MJ/m^2)), Smoke Production Rate (SPR, (m^2/s)), Total Smoke Release (TSR, (m^2/m^2)) and final residue (%). The test was repeated 3 times for each formulation and the experimental error was calculated as the standard deviation (σ). Before the test, specimens were stored in a climatic chamber (23.0 ± 0.1 °C, 50.0 ± 0.1%RH) for 48 h.

Raman spectra of post-combustion residues were performed on an InVia Raman Microscope (Renishaw S.p.A., Torino, Italy) equipped with a 514 nm laser and a Leica DM 2500 optical microscope (Leica Microsystems S.r.l., Milano, Italy).

3. Results and discussion

3.1. CoPECs formulation and fiber network morphology

The fabrication process of GEL/CNF CoPECs is detailed in Fig. S1a. Firstly, the effect of the pH of gelatin solution on the formation of the polyelectrolyte complex was investigated. Gelatin solutions were prepared at different pH, from 4 to 8, mixed with the CNF suspension and stirred for 20 min. Subsequently, the complexes were centrifuged in order to compact them and obtain a gel. Gelatin is a polyampholyte and

due to its nature is able to interact with both negatively and positively charged polyelectrolytes depending on the pH of the solution [50]. At pH less than isoelectric point (pI) gelatin becomes positively charged due to the protonation of amino group otherwise it is negatively charged [51]. From visual observation, at pH higher than 6 and above the isoelectric point, little to no complexation occurred and it was not possible to obtain a CoPECs gel after centrifuging the mixture (Fig. S1b). This is due to the fact that both polyelectrolytes are negatively charged in basic conditions and no electrostatic complexation occurs. Below the isoelectric point, pH equal to or lower than 6, a complexation reaction occurs and the so formed PECs can be further compacted by centrifugal forces into a gel (Fig. 2a). The compacted PECs were then freeze-dried in order to obtain lightweight samples having a density of about 30 kg/m^3 (Fig. 2b). Pure gelatin freeze-dried samples having the same density were also prepared at different pH and considered as reference samples. Upon freeze-drying the CoPECs yield a porous structure with cell walls clearly displaying nanocellulose bundles embedded in a gelatin matrix as pointed out by the arrow in Fig. 2c). Fig. 2d displays the ATR-FTIR spectra of neat GEL and CNF and of GEL/CNF complexes obtained varying the pH of gelatin solution. IR spectrum of neat gelatin shows the characteristic signals linked to the different vibration mode of the peptide bond. The large band between 3500 – 3200 cm^{-1} could be ascribed to Amide A (N—H stretching vibration) that overlaps with the broad band linked to the O—H stretching vibration of water molecules. The signals at 1630 cm^{-1}, 1550 cm^{-1}, 1240 cm^{-1} are associated with C═O stretching vibration (Amide I), N—H bending vibration (Amide II) and C—N stretching vibration (Amide III), respectively [52–54]. Pure CNF spectrum shows a broad band centered at 3340 cm^{-1} linked to O—H stretching. C—H_2 groups are found at 2850 cm^{-1}. Carboxylate group (COO^- asymmetric stretching) displays a signal at 1610 cm^{-1} while at 1060 cm^{-1} is visible the main peak ascribed to the C—O—C glycosidic bond [40,55]. The GEL/CNF CoPECs show the characteristic peaks of both components. Interestingly, the relative intensities of the main GEL and CNF peaks change with the pH thus suggesting different relative compositions of the PECs. The IR spectra of the supernatant phase removed after centrifuging (Fig. S2) evidenced the characteristic signals of GEL indicating that only a portion of GEL remained in the supernatant phase whereas the CNF was completely included in the CoPECs. Given the performed IR characterization, it can be concluded that the CoPECs produced at pH 6 are the richer in GEL and CNF content.

Compression stress-strain data, densities and calculated compression moduli are reported in Table S2. As can be observed from the data, at pH 6 pure gelatin has a stress at 10% strain higher than the one measured at pH 4. This behavior can be ascribed to the fact that, in acidic conditions, the gelatin chains are mostly positively charged so that, upon freeze-drying, the repulsive forces prevent the orientation of the GEL chains into well-organized structure. On the contrary, when the pH is close to the isoelectric point, a more compact and stronger configuration can be reached upon freeze drying [56,57]. The addition of CNF to the PECs promoted the formation of intermolecular hydrogen bonds and hydrophobic interactions with GEL while introducing bridging structures between molecules and therefore improving the foam stiffness [58,59]. As observed for neat GEL, CoPECs produced at pH 6 show the best properties in terms of compressive modulus and compressive stress at 10% deformation (Fig. 2d). These latter CoPECs were therefore selected as matrix for the inclusion of collagen fibers. To this aim, GELpH6/CNF complex gel was mixed mechanically with the collagen fibers at different weight ratios (i.e., 50/50 and 25/75) and freeze-dried in order to obtain porous fiber networks at two different densities (50 and 90 kg/m^3) (Fig. S3).

The produced fiber networks are robust and can be easily handled without damaging them (Fig. S4a). Conversely, it is worth to notice that it is not feasible to make a comparable material made only with the fibers because after freeze-drying there is no network formation, the structure is very brittle and easily collapses upon being removed from the mold (Fig. S4b). The structure of the prepared fiber networks was investigated by SEM (Fig. 3). The morphology of neat fibers was also investigated (Fig. S5). Collagen fibers displayed an irregular shape likely due to their sources. Indeed, being recovered as waste from the tannery process, these fibers exhibit a heterogeneous distribution in dimensions. It is visible a hierarchical structure that consists of collagen fibrils, at the nanometric scale, that self-arranged into fibers that are bound in a longitudinal arrangement into fiber bundles [60,61].

As far as the fiber networks are concerned, the collected SEM pictures, reported in Fig. 3, revealed the formation of a 3D structure where the fibers are held together by the GEL/CNF CoPECs. During freezing, the growth of ice crystal pushes the fibers and the matrix together. Upon sublimation, the ice crystals left behind pores and the presence of the PEC is essential to link the fibers and confer structural integrity. The interpenetration of the coated fibers contributed to make entanglements

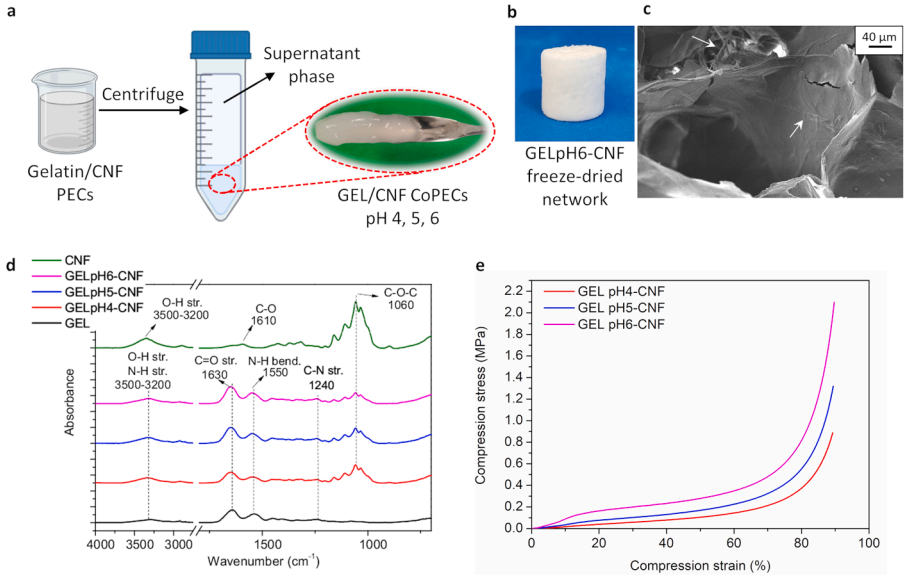


Fig. 2. Production and characterization of polyelectrolyte complexes: (a) Schematic representation of the procedure employed to produce CoPECs; (b) Digital photo of the GELpH6-CNF gel after freeze-drying; (c) SEM micrograph of the freeze-dried pH6 CoPECs; (d) ATR spectra of pure components and GEL-CNF complexes at different pH; (e) Compression stress-strain curves for the freeze-dried CoPECs at different pH.

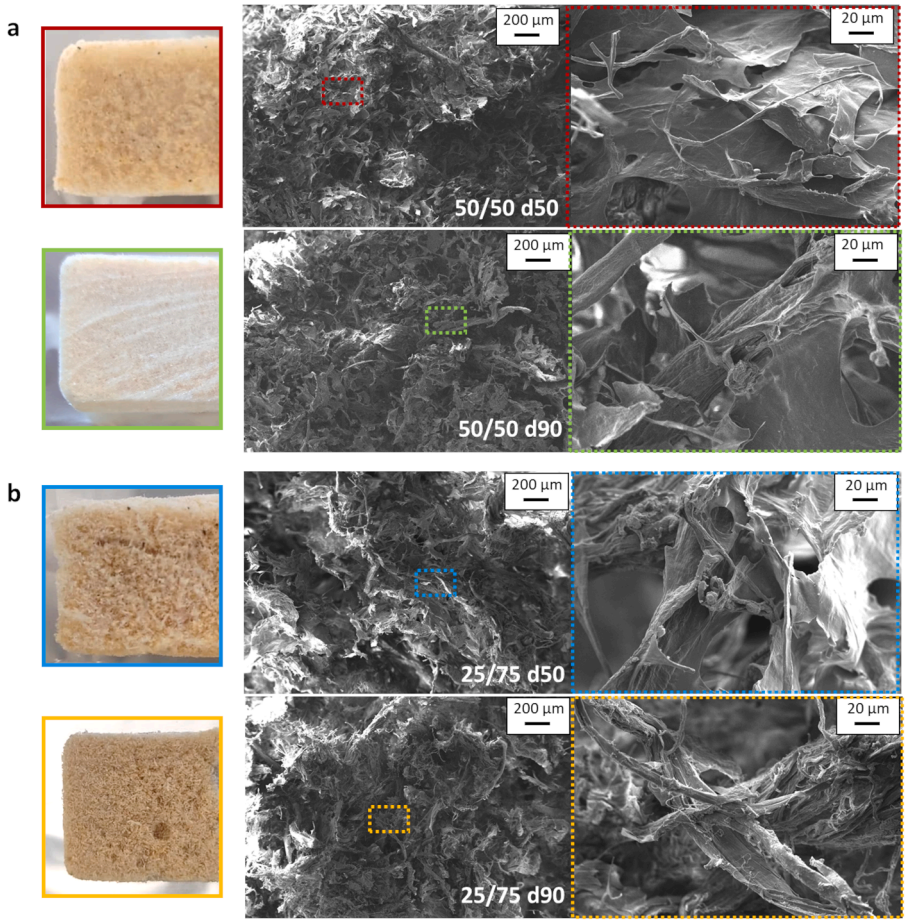


Fig. 3. Digital photos and SEM images at different magnifications of 50 and 90 kg/m^3 fiber networks produced at different compositions: (a) 50/50, (b) 25/75.

and joints between the fibers, keeping them together and creating a 3D network with structural integrity [62]. A difference in the microstructure between the two selected compositions is clearly observable. In the 50/50 samples (Fig. 3a) the fibers were embedded into the GEL/CNF matrix resulting in a good adhesion between the matrix and the fibers. Conversely, for the 25/75 compositions (Fig. 3b), due to the higher content of fibers, the CoPECs mostly act as a glue joining together the fibers and improving fiber-fiber interactions.

3.2. Mechanical and thermal insulation properties

The mechanical properties have been evaluated by compression tests while the thermal insulation properties have been assessed by measuring the thermal conductivity. Fig. 4 shows compression stress-strain curves for both 50/50 and 25/75 compositions at different densities, the evaluated compression stress at 10% strain and the comparison of the measured thermal conductivity values with reference materials from literature background [63–66].

Upon compression, all the samples show a linear behavior at very low deformation (< 2%), then the samples displayed a progressive collapse of the structure reaching a densification stage at higher deformation. The values of the compression modulus calculated and the compression stress reached at 10% of strain are reported in Table S3. The mechanical properties, for both compositions, scale with the density with d90 samples being more rigid than d50 samples (Fig. 4a). In addition, as reported in Fig. 4c, the stress measured at 10% strain further highlights a different trend linked to composition. For example, 0.102 ± 0.012 and 0.018 ± 0.003 MPa are required to achieve a 10% compressive strain for 50/50 d90 and 25/75 d90 networks, respectively, with a similar trend also observed for d50 samples. From a composition point of view, increasing the fibers content produced a decrease in the mechanical strength. This suggests that the CoPECs matrix as the main component contributing to the stiffness of the networks. This is in accordance with the microstructure observed by SEM investigation. Indeed, for the 50/50 composition fibers are embedded inside a continuous matrix while for the 25/75 composition the GEL/CNF complex just acts like a coating around the fibers making joints between the fibers thus producing a reduced effect on the compressive strength of the material.

The thermal conductivity values for materials in this work fall between 0.043 ± 0.002 and 0.063 ± 0.001 W/(m·K), which is in line with typical thermal conductivity of insulation materials made with natural fibers that are reported in the range of 0.03 and 0.1 W/(m·K) [63]. The obtained values are below 0.065 W/(m·K) that is considered the upper limit for thermal insulation applications [67]. Interestingly, the thermal conductivity of the foams decreases by increasing the density (i.e., the lowest value is achieved by 50/50 d90, Table S3). This behavior could be ascribed to the fact that in fiber based porous materials the apparent thermal conductivity actually depends on the combination of the different heat transfer mechanisms, namely heat conduction within the solid network, gas phase convection within the pores and radiative heat transfer across the pores [68]. For the materials under study, the increase in density is associated to a reduction of the pore size (Fig. 3), which may reduce the convective and radiative terms to the point of outweighing the expected increase in the conductive term as density increases [69]. Fig. 4d shows a comparison between the thermal conductivity values obtained in this work to other materials from literature background. The measured values are higher than those of traditional petroleum-derived porous materials (PU and EPS) but are comparable to those of natural-based porous materials and fiberboards.

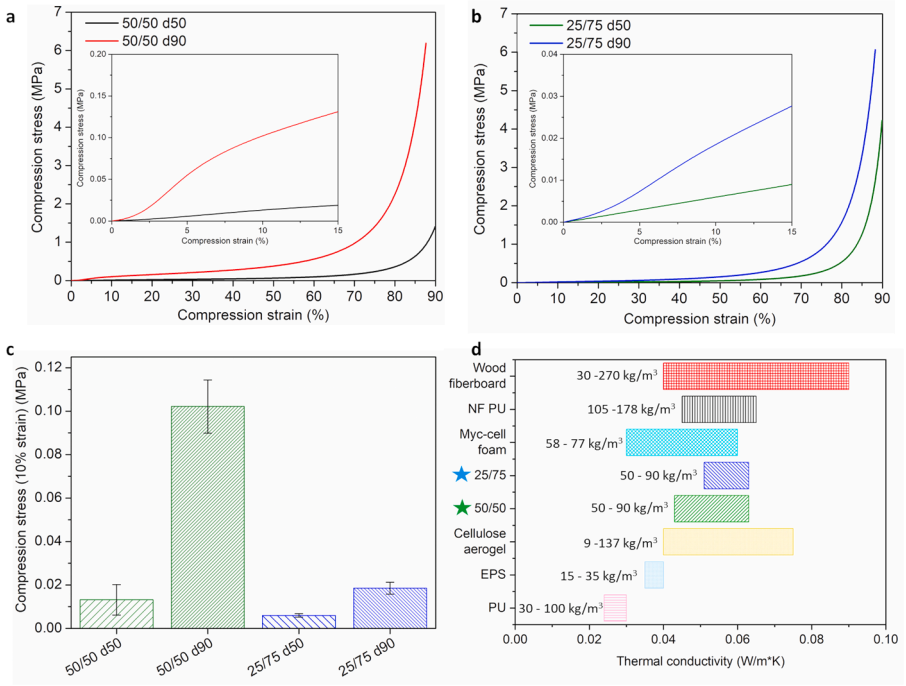


Fig. 4. Fiber networks characterization: Compression stress-strain curves for (a) 50/50 samples, (b) 25/75 samples with a magnification in the compression range of 0–20%; (c) Comparison of the compression stress calculated at 10% strain of the samples prepared; (d) Comparison of the thermal conductivity of different materials, PU: polyurethane foam (30 – 100 kg/m^3), EPS: expanded polystyrene foam (15 – 35 kg/m^3), Cellulose aerogel: regenerated cellulose aerogel (9 – 137 kg/m^3), Myc-cell foam: Mycelium-Cellulose foam (58 – 77 kg/m^3), NF PU: polyurethane foam reinforced with natural fibers (105 – 178 kg/m^3), Wood fiberboard (30 – 270 kg/m^3).

3.3. *Flame retardant properties*

Flammability and cone calorimetry test were performed in order to assess the flame retardancy properties of the prepared fiber networks. The first evaluates the reaction of a material to the application of a small flame simulating a possible ignition source, the second is used to establish the behavior of a material when exposed to a heat flux typically found during the early stages of a fire [70,71]. Fig. 5 shows the snapshots taken during the flammability test in the horizontal and vertical configuration of all the samples and residue values at the end of the test.

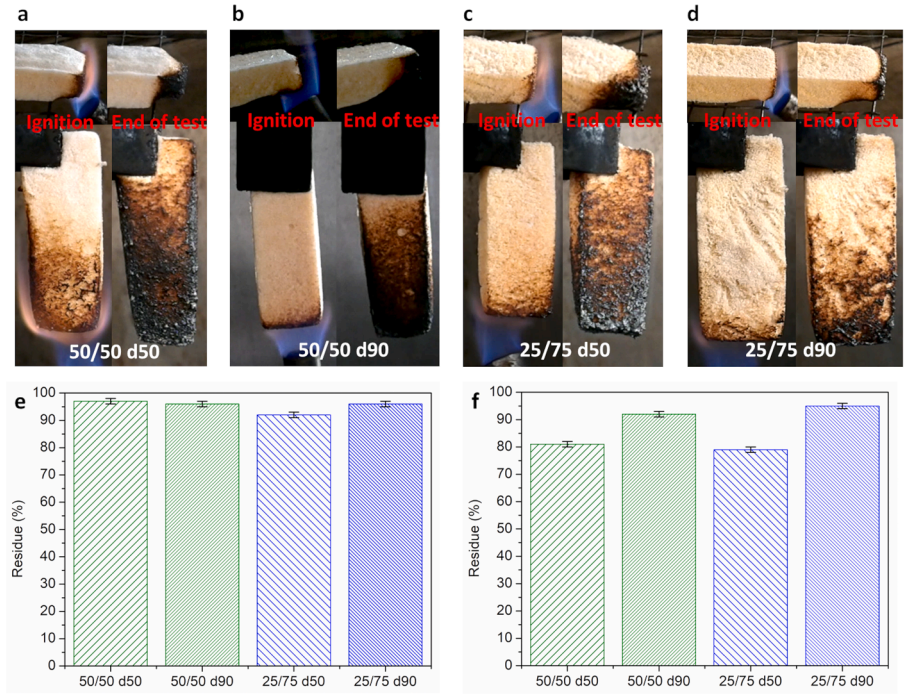


Fig. 5. Flammability of the prepared samples: Snapshots taken during the flammability test in the horizontal and vertical configuration for (a) 50/50 d50, (b) 50/50 d90, (c) 25/75 d50, (d) 25/75 d90; Residue (%) at the end of the test in (e) horizontal configuration (f) vertical configuration.

Table S4 and Table S5 display the numerical data of flammability and cone calorimetry test for all samples tested.

Flammability was first tested in the horizontal configuration. All the tested samples did not ignite and the flame immediately self-extinguished after the removal of the methane flame with an after-flame time of 0 s thus suggesting a non-igniting behavior. This behavior occurred at each flame application. At the end of the test, the samples displayed little to no damage yielding residue values above 90% (Table S4). The flammability in vertical configuration was also performed. In this configuration the samples are tested in a more severe condition if compared to the horizontal one. All samples showed a self-extinguishing behavior but for both d50 samples the flames reached the clamp during the second flame application and then self-extinguished immediately after the removal of the methane flame. As reported in Fig. 5, d50 samples display extensive char formation on most of the exposed surface while for denser and fiber-rich samples (i.e., 25/75 d90) the portion of sample that was damaged by the flame is reduced. Digital images of the residue cross-sections revealed that only the surface was actually damaged by the flame while the internal part of the sample was not damaged (Fig. S6). The best results were obtained by 25/75 d90 samples which showed no flame propagation and immediately self-extinguished after each methane flame application therefore exhibiting a non-igniting behavior also in vertical configuration.

In order to provide complementary fire safety data, cone calorimetry tests were performed to investigate the sample reaction when exposed to a 50 kW/m^2 heat flux, simulating a developed fire scenario [71]. Fig. 6 displays digital images taken during the cone calorimetry test, cone calorimetry HRR and average rate of heat emission (ARHE) as a function of time plot, pkHRR, THR and TSR values for the samples tested and a comparison with the literature background [72–76]. Fig. S7 shows digital images of the residue of the samples taken after cone calorimetry test.

Upon the exposure to a heat flux the material starts decomposing, releasing volatile gases that lead to sample ignition and flaming combustion (Fig. 6a). For 50/50 samples ignition occurs after an average of 10 s while for 25/75 samples the time of ignition increases to 40 s. This suggests the ignition being piloted by the amount of CoPECs matrix. During combustion, extensive charring of the samples occurs, allowing the maintenance of their structural integrity at the end of the test. As displayed by HRR plots, for all tested samples the peak of heat release rate (pkHRR) is reached right after ignition and then the HRR values gradually decrease till flaming combustion ceases. pkHRR values display a decreasing trend as the amount of collagen-rich fibers increases (e.g., 152 ± 19 kW/m^2 vs 118 ± 3 kW/m^2 for 50/50 d90 and 25/75 d90, respectively). THR increases with the increase in density for both compositions (e.g., from 9.7 ± 0.4 to 16.9 ± 1.4 MJ/m^2 for 50/50 d50 and 50/50 d90, respectively), while it decreases as the fiber content is increased at constant density (e.g., from 9.7 ± 0.4 to 4.4 ± 0.4 MJ/m^2 for 50/50 d50 and 25/75 d50, respectively). Conversely, the total smoke release (TSR) increases as the fiber content increases as demonstrated, for example, by d90 samples that yielded TSR values of 187 ± 12 and 241 ± 58 m^2/m^2 for 50/50 and 25/75 compositions, respectively. The residue (%) at the end of the test increases with the increase of the density of the network (Table S5). The average rate of heat emission (ARHE) is reported in Fig. 6f. This parameter, defined as the cumulative heat emission divided by time, and its peak value, the maximum average

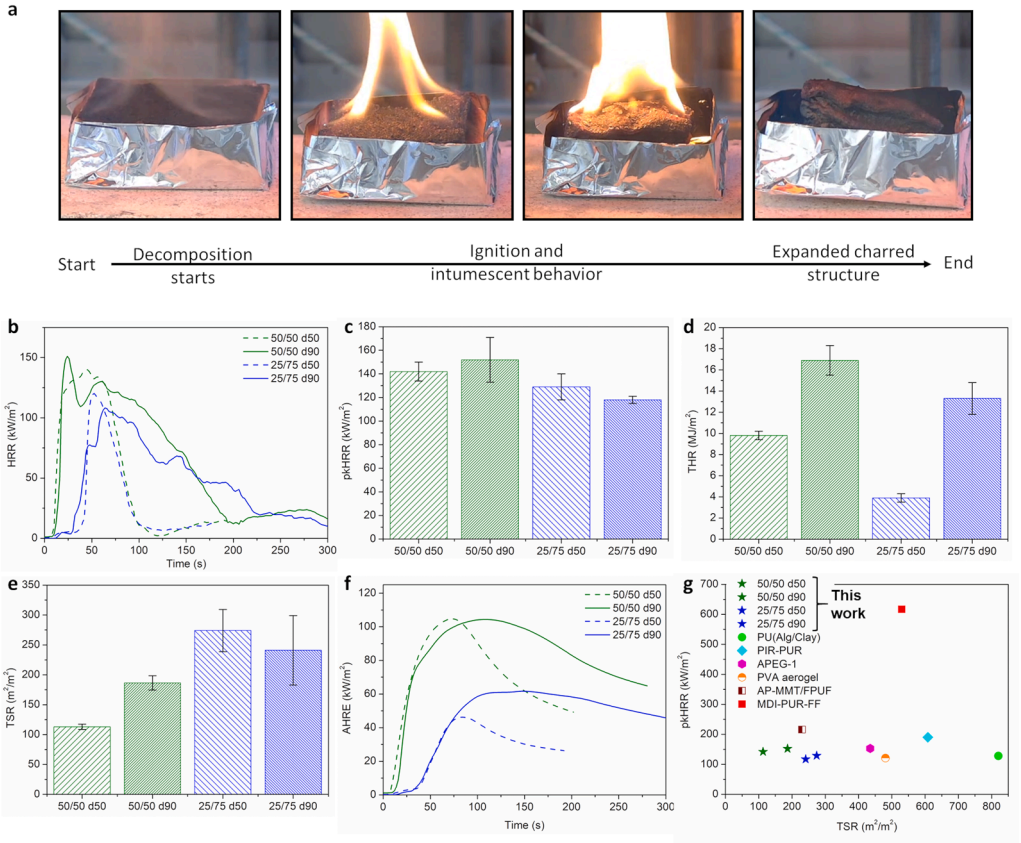


Fig. 6. Forced combustion characterization. (a) Snapshots taken during cone calorimetry test; (b) Cone calorimetry plot of heat released rate (HRR) as a function of time; (c - e) Peak of heat released rate (pkHRR), Total heat released (THR) and total smoke released (TSR) measured for the samples tested, (f) Average rate of heat emission (ARHE) as a function of time, (g) pkHRR and TSR of prepared samples compared to those of other porous materials from literature background, PU(Alg/Clay): PU foam with surface coating made with alginate and clay aerogel; PIR-PUR: polyisocyanurate-polyurethane foam; APEG-1: PIR-PUR foam with ammonium phosphate and expandable graphite; PVA aerogel: poly(vinyl alcohol) composite aerogel with ammonium polyphosphate and chitosan; AP-MMT/FPUF: PU foam coated with phytic acid and clay; MDI-PUR-FF: commercial PU foam.

rate of heat emission (MARHE), can be considered a reliable indicator of the propensity of fire development under real scale condition [77]. In particular, the MARHE value is a key fire safety parameter commonly used for regulatory assessments across various application sectors, such as transportation [78]. ARHE plots reported in Fig. 6f remain below the 110 kW/m^2 value indicating a reduced propensity to fire development. For comparison, rigid polyurethane/polyisocyanurate foams based on bio-polyols would fall in the 200–300 kW/m^2 range [79] . Samples characterized by high fiber content show the best performances with plots and MARHE values (see Table S5) that remain below 90 kW/m^2, that is often considered as the threshold value for many applications (e.g., building) [80]. The flame retardancy performance of the prepared materials is further highlighted by a comparison with the pkHRR and TSR values (evaluated under 50 kW/m^2) of flame retardant porous materials from the literature background (Fig. 6g). The collagen-based networks developed in this paper were located in the region of low pkHRR and TSR, clearly highlighting their fire safety properties.

3.4. Post combustion residue analysis

The residues collected after cone calorimetry test were investigated by SEM and Raman spectroscopy. Fig. 7 displays digital images, SEM micrographs of cross-sections and Raman spectra of 50/50 d50 and 25/75 d90 residues (i.e., the two extremes in terms of composition and density). Fig. S8 displays the digital photos and SEM images of the 50/50 d90 and 25/75 d50 networks. Raman spectra of the same composition are reported in Fig. S9.

After combustion, the fiber networks yielded a self-standing charred residue that can be easily handled. From the digital photos is visible a porosity at the macroscopic level while a microporosity is evidenced by SEM micrographs at high magnifications. Raman spectra highlight the formation of G and D bands that are characteristic signals typically found in graphene and graphene related materials [81]. The former, at 1590 cm^{-1}, is related to the stretching of sp^2 carbons while the latter, at 1350 cm^{-1}, is related to the presence of defects (e.g., edges, curvature and inclusions) close to sp^2 carbon rings. For combustion residues, these two bands are often broadened with respect to those found in pristine graphitic materials due to the complexity of the charred structures produced during thermal decomposition [82]. The evaluation of the ratio between the area underneath the G and D bands (G_A and D_A, respectively) provide information about the quality of the aromatic structure [83]. The measured spectra showed D_A/G_A ratios between 2.4 and 2.7, in agreement with those reported in the literature for graphene oxide-containing combustion residues [84]. These results suggest the formation, during combustion, of a carbonaceous char with partially graphitic structure [62]. These results are ascribed to the inherent intumescent feature and char forming characteristics of both the employed CoPECs and the collagen fibers. As visible in Fig. 6a, when exposed to a heat flux, both the CoPECs and the collagen fibers start decomposing releasing volatiles. Upon ignition, the release of CO_2, NH_3 and water from both the fibers and the gelatin contained into the matrix promotes the expansion of the network, leading to the formation of an intumescent, charred layer on the surface of the burning samples [24,85,86]. At the same time, the CNF embedded within the matrix also starts decomposing producing extensive charring that confer structural integrity to the expanded structure of the network [87,88]. The formation of an expanded network at the flame interface limits the release of volatile products while also reducing the heat transfer. These combined effects eventually lead to the self-extinguished behavior observed during flammability test along with the low heat and smoke production rates observed by cone calorimetry.

4. Conclusion

In this work, in an effort to mitigate the environmental impact of the leather industry, collagen-rich fibers from tannery wastes have been upcycled into lightweight and flame retardant porous fiber networks by exploiting the unique set of properties and processing versatility of bio-sourced PECs. Gelatin and carboxymethylated cellulose nanofibers were selected as building blocks for the production of CoPECs to be used as matrix capable of conferring structural integrity to the fiber networks. The effects of the pH complexing conditions on the dry CoPECs mechanical properties were investigated. pH 6 was found to promote efficient interactions between gelatin and CNF that resulted in optimal mechanical properties of freeze dried CoPECs. This enabled the use of the CoPECs for the preparation of lightweight fiber networks encompassing collagen-rich fibers with different compositions (50/50 and 25/75 matrix/fiber ratio) and densities (50 and 90 kg/m^3). SEM observations pointed out that for the 50/50 composition the fibers were incorporated into the PECs matrix while, in the 25/75, the CoPECs mainly acted as a glue between them, greatly improving fiber-fiber interactions. Such microstructure affected the mechanical properties of the network with the 50/50 composition yielding higher compressive stresses if compared to the 25/75. Density also influenced mechanical properties with d90 specimens for both compositions exhibiting improved stiffness. These results underlined the fact that the strong interaction achieved in the CoPECs significantly contributed to the mechanical strength of the fiber networks. Thermal conductivities values were found to be in the 0.043 - 0.063 W/m·K range that is below the threshold commonly employed for materials in insulating application. From the fire safety point of view, all prepared networks prevented flame propagation during horizontal flammability tests while only the networks prepared at high fiber content displayed a self-extinguishing behavior in vertical configuration. Forced combustion test performed at 50 kW/m^2 pointed

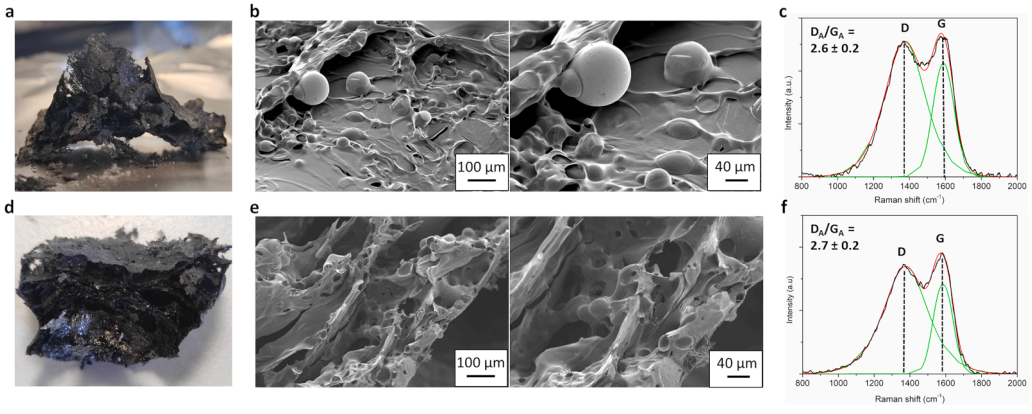


Fig. 7. Analysis of the residues of 50/50 d50 (first row, a-c) and 25/75 d90 (second row, c-f) networks collected after cone calorimetry tests: digital photos of the cross-section of the residues (a, d), SEM micrographs (b, e) and Raman spectra (c, f).

out how denser and fiber rich samples can yield very low peaks of heat release rate (i.e. pkHRR 118 ± 3 kW/m^2 for 25/75 d90 sample) whereas lighter samples prepared with an equal amount of CoPECs and fiber achieve the best performance in smoke release (i.e. TSR 113 ± 4 m^2/m^2 for 50/50 d50 sample). A comparison with the literature background further highlights how these materials can rival with high performing solutions commonly employed by the state of the art. These outstanding results were mainly ascribed to the inherent flame retardancy of collagen fibers. The 90 kg/m^3 (25/75) fiber network displays the optimal balance between the amount fibers upcycled and the achieved mechanical, thermal insulating and fire safety properties therefore constituting a sustainable and high performing alternative to commonly employed materials that are typically based on non-renewable resources. In conclusion, the proposed work discloses a viable strategy for the use of CoPECs and collagen-rich fibers for the production of sustainable and functional materials for transportation or building applications.

CRediT authorship contribution statement

Lorenza Abbà: Writing – original draft, Visualization, Validation, Investigation, Conceptualization. **Rosario Mascolo:** Writing – review & editing, Resources. **Claudia Florio:** Writing – review & editing, Funding acquisition. **Alberto Fina:** Writing – review & editing, Funding acquisition. **Federico Carosio:** Writing – review & editing, Visualization, Supervision, Project administration, Conceptualization.

Declaration of competing interest

The authors declare that they have no known competing financial interests or personal relationships that could have appeared to influence the work reported in this paper.

Acknowledgements

This study was carried out within the MICS (Made in Italy–Circular and Sustainable) Extended Partnership and received funding from the European Union Next-Generation EU (PIANO NAZIONALE DI RIPRESA E RESILIENZA (PNRR) – MISSIONE 4 COMPONENTE 2, INVESTIMENTO 1.3 –D.D. 1551.11-10-2022, PE00000004). This manuscript reflects only the authors' views and opinions, neither the European Union nor the European Commission can be considered responsible for them.

Supplementary materials

Supplementary material associated with this article can be found, in the online version, at doi:10.1016/j.polymdegradstab.2026.112300.

Data availability

Data will be made available on request.

References

[1] M. Shen, et al., Are biodegradable plastics a promising solution to solve the global plastic pollution? Environ. Pollut. 263 (2020) 114469.
[2] M. Ramesh, K. Palanikumar, K.H. Reddy, Plant fibre based bio-composites: sustainable and renewable green materials, Renew. Sustain. Energy Rev. 79 (2017) 558–584.
[3] H. Ku, et al., A review on the tensile properties of natural fiber reinforced polymer composites, Compos. B: Eng. 42 (4) (2011) 856–873.
[4] A. Teklay, et al., Preparation of value added composite boards using finished leather waste and plant fibers—a waste utilization effort in Ethiopia, Clean Technol. Environ. Policy 19 (2017).
[5] Y. Wang, et al., Advanced collagen nanofibers-based functional bio-composites for high-value utilization of leather: a review, J. Sci.: Adv. Mater. Devices 6 (2) (2021) 153–166.
[6] K. Chojnacka, et al., Progress in sustainable technologies of leather wastes valorization as solutions for the circular economy, J. Clean. Prod. 313 (2021) 127902.
[7] V. Muralidharan, P. Saravanan, B. Madhan, Turning problem into possibility: a comprehensive review on leather solid waste intra-valorization attempts for leather processing, J. Clean. Prod. 367 (2022) 133021.
[8] C.R. China, et al., Alternative tanning technologies and their suitability in curbing environmental pollution from the leather industry: a comprehensive review, Chemosphere 254 (2020) 126804.
[9] Regulation (EC) No 1069/2009 of the European Parliament and of the Council of 21 October 2009 laying down health rules as regards animal by-products and derived products not intended for human consumption and repealing Regulation (EC) No 1774/2002 (Animal by-products Regulation). 2009.
[10] J. Kanagaraj, et al., Eco-friendly waste management strategies for greener environment towards sustainable development in leather industry: a comprehensive review, J. Clean. Prod. 89 (2015) 1–17.
[11] N. Venkatesan, A. Krishna, N.N. Fathima, Leather solid waste derived activated carbon as a potential material for various applications: a review, J. Anal. Appl. Pyrolysis 176 (2023) 106249.
[12] S. Rethinam, et al., Recycling of finished leather wastes: a novel approach, Clean Technol. Environ. Policy 17 (2014) 187–197.
[13] S. Selvaraj, et al., Chromium containing leather trimmings valorization: sustainable sound absorber from collagen hydrolysate intercalated electrospun nanofibers, J. Hazard. Mater. 405 (2021) 124231.
[14] G. Bufalo, et al., Principles of minimal wrecking and maximum separation of solid waste to innovate tanning industries and reduce their environmental impact: the case of paperboard manufacture, J. Clean. Prod. 174 (2018) 324–332.
[15] V. Ottani, et al., Hierarchical structures in fibrillar collagens, Micron 33 (7-8) (2002) 587–596.
[16] J. Li, et al., Leather-like hierarchical porous composites with outstanding electromagnetic interference shielding effectiveness and durability, Compos. B: Eng. 225 (2021) 109272.
[17] M. Mendrycka, M. Kowalska, W. Myjak, Assessment of the properties of emulsions containing different amounts of collagen derived from calf skins, Mater. Plast. 53 (1) (2016) 113–118.
[18] R. Murali, et al., Hybrid biodegradable films from collagenous wastes and natural polymers for biomedical applications, Waste Biomass Valorization 2 (2011) 323–335.
[19] J.R. Rao, et al., Green route for the utilization of chrome shavings (chromium-containing solid waste) in tanning industry, Environ. Sci. Technol. 36 (6) (2002) 1372–1376.
[20] R. Lazău, et al., Ceramic pigments with chromium content from leather wastes, J. Eur. Ceram. Soc. 27 (2-3) (2007) 1899–1903.
[21] L. Chabaane, et al., Immobilization of vegetable tannins on tannery chrome shavings and their use for the removal of hexavalent chromium from contaminated water, Chem. Eng. J. 174 (1) (2011) 310–317.
[22] L.C. Oliveira, et al., Removal of organic dyes using Cr-containing activated carbon prepared from leather waste, J. Hazard. Mater. 192 (3) (2011) 1094–1099.
[23] G.D. Ribeiro, et al., Sustainable construction materials for low-cost housing: thermal insulation potential of expanded SBR composites with leather waste, J. Mater. Res. Technol. 30 (2024) 5590–5604.
[24] W. Xu, et al., Effects of collagen fiber addition on the combustion and thermal stability of natural rubber, J. Leather Sci. Eng. 2 (2020) 1–10.
[25] T. Zhang, et al., Leather solid waste/poly (vinyl alcohol)/polyaniline aerogel with mechanical robustness, flame retardancy, and enhanced electromagnetic interference shielding, ACS Appl. Mater. Interfaces 13 (9) (2021) 11332–11343.
[26] C. Chen, et al., Lightweight, thermally insulating, fire-proof graphite-cellulose foam, Adv. Funct. Mater. 33 (6) (2023) 2204219.
[27] X. Zhao, et al., A scalable high-porosity wood for sound absorption and thermal insulation, Nat. Sustain. 6 (3) (2023) 306–315.
[28] N.V. Gama, A. Ferreira, A. Barros-Timmons, Polyurethane foams: past, present, and future. Materials, MDPI AG, 2018.
[29] C.G. Otoni, et al., Charge matters: electrostatic complexation As a green approach to assemble advanced functional materials, ACS Omega 5 (3) (2020) 1296–1304.
[30] X. Liu, H. Peng, Q. Zhao, Perspective on the processing and functionalities of solid-State polyelectrolyte complexes, Macromolecules (2025).
[31] B.P. Das, M. Tsianou, From polyelectrolyte complexes to polyelectrolyte multilayers: electrostatic assembly, nanostructure, dynamics, and functional properties, Adv. Colloid Interface Sci. 244 (2017) 71–89.
[32] Q. Wang, J.B. Schlenoff, The polyelectrolyte Complex/coacervate continuum, Macromolecules 47 (9) (2014) 3108–3116.
[33] O. Mermut, C.J. Barrett, Effects of charge density and counterions on the assembly of polyelectrolyte multilayers, J. Phys. Chem. B 107 (11) (2003) 2525–2530.
[34] G. Rydzek, et al., pH-responsive saloplastics based on weak polyelectrolytes: from molecular processes to material scale properties, Macromolecules 51 (12) (2018) 4424–4434.
[35] C.H. Porcel, J.B. Schlenoff, Compact polyelectrolyte complexes:"saloplastic" candidates for biomaterials, Biomacromolecules 10 (11) (2009) 2968–2975.
[36] R.F. Shamoun, A. Reisch, J.B. Schlenoff, Extruded saloplastic polyelectrolyte complexes, Adv. Funct. Mater. 22 (9) (2012) 1923–1931.
[37] S. Lindhoud, W.M. de Vos, Hot-pressed polyelectrolyte complexes as novel alkaline stable monovalent-ion selective anion exchange membranes, J. Colloid Interface Sci. 593 (2021) 11–20.
[38] R.R. Costa, et al., Compact saloplastic membranes of natural polysaccharides for soft tissue engineering, Chem. Mater. 27 (21) (2015) 7490–7502.

[39] P. Schaaf, J.B. Schlenoff, Saloplastics: processing compact polyelectrolyte complexes, Adv. Mater. 27 (15) (2015) 2420–2432.
[40] F. Carosio, et al., Layer-by-layer-assembled chitosan/phosphorylated cellulose nanofibrils as a bio-based and flame protecting nano-exoskeleton on PU foams, Carbohydr. Polym. 202 (2018) 479–487.
[41] A. Ayoub, et al., Novel hemicellulose–Chitosan biosorbent for water desalination and heavy metal removal, ACS Sustain. Chem. Eng. 1 (2013) 1102–1109.
[42] F. Luo, et al., Oppositely charged polyelectrolytes form tough, self-healing, and rebuildable hydrogels, Adv. Mater. 27 (2015).
[43] S. Robertis, et al., Advances in oral controlled drug delivery: the role of drug-polymer and interpolymer non-covalent interactions, Expert Opin. Drug Deliv. 12 (2014) 1–13.
[44] H.C.L. de Oliveira, J.L.C. Fonseca, M.R. Pereira, Chitosan-poly(acrylic acid) polyelectrolyte complex membranes: preparation, characterization and permeability studies, J. Biomater. Sci. Polym. Ed. 19 (2) (2012) 143–160.
[45] R.J. Smith, C.T. Long, J.C. Grunlan, Transparent polyelectrolyte complex thin films with ultralow oxygen transmission rate, Langmuir 34 (37) (2018) 11086–11091.
[46] L. Maddalena, et al., Cellulose nanocrystals polyelectrolyte complexes as flame retardant treatment for cotton fabrics, Polym. Degrad. Stab. 220 (2024) 110646.
[47] J. Fu, Q. Wang, J.B. Schlenoff, Extruded superparamagnetic saloplastic polyelectrolyte nanocomposites, ACS Appl. Mater. Interfaces 7 (1) (2014) 895–901.
[48] Q. Zhao, et al., A novel method for fabricating polyelectrolyte complex/inorganic nanohybrid membranes with high isopropanol dehydration performance, J. Membr. Sci. - J Membr. Sci. 345 (2009) 233–241.
[49] R. Mascolo, et al., Estimation of particle dimension and particle size distribution (PSD) of ground leather using a digital image processing method (DIP), J. Am. Leather Chem. Assoc. 120 (9) (2025).
[50] S.R. Derkach, N.G. Voron'ko, Y.A. Kuchina, Intermolecular interactions in the formation of polysaccharide-gelatin complexes: a spectroscopic study, Polymers 14 (14) (2022) 2777.
[51] Y. Zhang, et al., Fabrication and characterization of complex coacervates utilizing gelatin and carboxymethyl starch, J. Sci. Food Agric. 104 (6) (2024) 3585–3593.
[52] D. Hashim, et al., Potential use of Fourier transform infrared spectroscopy for differentiation of bovine and porcine gelatins, Food Chem. 118 (3) (2010) 856–860.
[53] A. Barth, Infrared spectroscopy of proteins, Biochim. Biophys. Acta (BBA) - Bioenerg. 1767 (9) (2007) 1073–1101.
[54] G. Socrates, Infrared and Raman characteristic group frequencies. Tables and Charts, 3 ed., wiley, 2001.
[55] S. Fujisawa, et al., Preparation and characterization of TEMPO-oxidized cellulose nanofibril films with free carboxyl groups, Carbohydr. Polym. 84 (1) (2011) 579–583.
[56] K.J. Goudie, et al., Investigation of the influence of pH on the properties and morphology of gelatin hydrogels, J. Polym. Sci. 61 (19) (2023) 2316–2332.
[57] Y. Lin, Z. Su, Layer-by-layer assembly of gelatin, J. Polym. Sci. B: Polym. Phys. 46 (12) (2008) 1252–1257.
[58] X. Feng, et al., Regulation mechanism of nanocellulose with different morphologies on the properties of low-oil gelatin emulsions: interfacial adsorption or network formation? Food Hydrocoll. 133 (2022) 107960.
[59] X. Feng, et al., Improvement of low-oil gelatin emulsions performance by adjusting the electrostatic interaction between gelatin and nanocellulose with different morphologies, Food Hydrocoll. 139 (2023) 108592.
[60] A. Battig, et al., Waste not, want not: the use of leather waste in flame retarded EVA, Mater. Des. 210 (2021) 110100.
[61] S. Li, et al., Scalable fabrication of collagen fiber-waterborne polyurethane foams with enhanced toughness and thermal insulation by constructing energy dissipation networks, J. Clean. Prod. 458 (2024) 142427.
[62] M. Marcioni, et al., Layer-by-Layer-coated cellulose fibers enable the production of porous, flame-retardant, and lightweight materials, ACS Appl. Mater. Interfaces 15 (30) (2023) 36811–36821.
[63] L.D. Hung Anh, Z. Pásztory, An overview of factors influencing thermal conductivity of building insulation materials. Journal of Building Engineering, Elsevier Ltd, 2021.
[64] H. Tu, et al., Recent progress in high-strength and robust regenerated cellulose materials, Adv. Mater. 33 (28) (2021) 2000682.
[65] P. Amstislavski, et al., Low-density, water-repellent, and thermally insulating cellulose-mycelium foams, Cellulose 31 (14) (2024) 8769–8785.
[66] H. Shao, et al., Renewable natural resources reinforced polyurethane foam for use of lightweight thermal insulation, Mater. Res. Express 7 (5) (2020).
[67] O. Dénes, I. Florea, D.L. Manea, Utilization of sheep wool as a building material, Procedia Manuf. 32 (2019) 236–241.
[68] Y.-L. He, T. Xie, Advances of thermal conductivity models of nanoscale silica aerogel insulation material, Appl. Therm. Eng. 81 (2015) 28–50.
[69] X. Lian, et al., Thermal conductivity analysis of natural fiber-derived porous thermal insulation materials, Int. J. Heat Mass Transf. 220 (2024) 124941.
[70] C. Lautenberger, J. Torero, C. Fernandez-Pello, 1 - understanding materials flammability, in: V.B. Apte (Ed.), Flammability Testing of Materials Used in Construction, Transport and Mining, Woodhead Publishing, 2006, pp. 1–21. Editor.
[71] B. Schartel, T.R. Hull, Development of fire-retarded materials—interpretation of cone calorimeter data, Fire Mater. 31 (2007) 327–354.
[72] C.C. Höhne, R. Hanich, E. Kroke, Intrinsic flame resistance of polyurethane flexible foams: unexpectedly low flammability without any flame retardant, Fire Mater. 42 (4) (2018) 394–402.
[73] H.B. Chen, et al., Highly efficient flame retardant polyurethane foam with alginate/clay aerogel coating, ACS Appl. Mater. Interfaces 8 (47) (2016) 32557–32564.
[74] X. Hu, D.M. Wang, Enhanced fire behavior of rigid polyurethane foam by intumescent flame retardants, J. Appl. Polym. Sci. 129 (2013).
[75] M. Luo, et al., Enhanced thermal insulation and flame-retardant properties of polyvinyl alcohol-based aerogels composited with ammonium polyphosphate and chitosan, Int. J. Polym. Sci. 2021 (2021) 1–11.
[76] P. Li, et al., Halogen-free coatings combined with the synergistic effect of phytic acid and montmorillonite for fire safety flexible polyurethane foam, Macromol. Mater. Eng. 307 (5) (2022).
[77] M. Sacristán, et al., Cone calorimetry studies of fire retardant soybean-oil-based copolymers containing silicon or boron: comparison of additive and reactive approaches, Polym. Degrad. Stab. 95 (7) (2010) 1269–1274.
[78] D. Hohenwarter, C. Fischer, M. Berger, Influence of 3D-printing on the flammability properties of railway applications using polycarbonate (PC) and polylactic acid (PLA), Probl. Kolejnictwa - Railw. Rep. 64 (2020) 99–107.
[79] M. Borowicz, J. Paciorek-Sadowska, M. Isbrandt, Analysis of the physicomechanical properties, flammability and smoke emission of rigid polyurethane/polyisocyanurate foams modified with bio-polyols based on white mustard oil with different content of sulfur atoms, J. Therm. Anal. Calorim. (2025).
[80] P. Koštial, Z.K. Jančíková, R. Frischer, Case study on fire resistance of sandwiches for means of transport, Coatings 11 (2) (2021) 207.
[81] A.C. Ferrari, D.M. Basko, Raman spectroscopy as a versatile tool for studying the properties of graphene, Nat. Nanotechnol. 8 (4) (2013) 235–246.
[82] M. Ayiania, et al., Microstructural analysis of nitrogen-doped char by Raman spectroscopy: raman shift analysis from first principles, Carbon 167 (2020) 559–574.
[83] B. Yu, et al., Enhanced thermal and flame retardant properties of flame-retardant-wrapped graphene/epoxy resin nanocomposites, J. Mater. Chem. A 3 (15) (2015) 8034–8044.
[84] F. Carosio, et al., Graphene oxide exoskeleton to produce self-extinguishing, nonignitable, and flame resistant flexible foams: a mechanically tough alternative to inorganic aerogels, Adv. Mater. Interfaces 5 (23) (2018) 1801288.
[85] C. Fang, et al., Nitrogen-containing gaseous products of chrome-tanned leather shavings during pyrolysis and combustion, Waste Manag. 78 (2018) 553–558.
[86] G. Sanchez-Olivares, et al., Utilizing leather fibers from industrial wastes as bio-filler to improve flame retardancy in polypropylene, J. Ind. Eng. Chem. 132 (2024) 148–160.
[87] F. Zhu, L. Chen, Q. Feng, Waste gelatin based layer by layer assembly for sustainable solution to cotton fabrics flame retardancy, Prog. Org. Coat. 163 (2022) 106688.
[88] A. Ait Benhamou, et al., Strong and flame-resistant nanocellulose sheets derived from agrowastes via a papermaking-assisted process, ACS Appl. Polym. Mater. 6 (5) (2024) 2763–2776.